

# Oscillations of non-slender tori in the external Hartle-Thorne geometry

Monika Matuszková,<sup>1,a</sup> Kateřina Klimovičová,<sup>1,b</sup>  
Gabriela Urbancová,<sup>1,c</sup> Debora Lančová,<sup>1,d</sup>  
Eva Šrámková<sup>1</sup> and Gabriel Török<sup>1</sup>

<sup>1</sup>Research Centre for Computational Physics and Data Processing,  
Institute of Physics, Silesian University in Opava, Bezručovo nám. 13,  
CZ-746 01 Opava, Czech Republic

<sup>a</sup>[monika.matuszkova@physics.slu.cz](mailto:monika.matuszkova@physics.slu.cz)

<sup>b</sup>[katerina.klimovicova@physics.slu.cz](mailto:katerina.klimovicova@physics.slu.cz)

<sup>c</sup>[gabriela.urbancova@physics.slu.cz](mailto:gabriela.urbancova@physics.slu.cz)

<sup>d</sup>[debora.lancova@physics.slu.cz](mailto:debora.lancova@physics.slu.cz)

## ABSTRACT

We examine the influence of the quadrupole moment of a slowly rotating neutron star on the oscillations of non-slender accretion tori. We apply previously developed methods to perform analytical calculations of frequencies of the radial epicyclic mode of a torus in the specific case of the Hartle-Thorne geometry. We present here our preliminary results and provide a brief comparison between the calculated frequencies and the frequencies previously obtained assuming both standard and linearized Kerr geometry. Finally, we shortly discuss the consequences for models of high-frequency quasi-periodic oscillations observed in low-mass X-ray binaries.

**Keywords:** neutron star – thick accretion disc – Hartle-Thorne metric

## 1 INTRODUCTION

Numerous interesting features have been discovered during the long history of X-ray observations of low-mass X-ray binaries (LMXBs). One of them is the fact that variability of the X-ray radiation coming from these sources occurs at frequencies in the order of up to hundreds of Hertz with the highest values reaching above 1.2 kHz. Even though the discovery of this rapid variability was made almost 30 years ago, to this day, there is no convincing explanation of its origin. The phenomenon is called the high-frequency quasi-periodic oscillations (HF QPOs) and many models have been proposed in the attempt to explain its nature (see, e.g., Török et al., 2016a; Kotrlová et al., 2020 and references therein).

It has been noticed that the HF QPOs frequencies are in the same order as those corresponding to orbital motion in the very close vicinity of a compact object, such as neutron

star (NS) or black hole (BH). This suggests that there is a relation between the QPO phenomenon and the physics behind the motion of matter close to the accreting object. Since positions of specific orbits in the accretion disk (such as its inner edge) and the associated orbital frequencies depend on the properties of the central object, there is a believe that it is possible to infer the compact object properties from the QPOs data.<sup>1</sup>

In the above context, several studies have focused on a possible relation between the QPOs and an oscillatory motion of an accretion torus formed in the innermost accretion region (Kluźniak and Abramowicz, 2001; Kluźniak et al., 2004; Abramowicz et al., 2003a,b; Rezzolla et al., 2003; Bursa, 2005; Török et al., 2005; Dönmez et al., 2011; Török et al., 2016a; de Avellar et al., 2018).

Straub and Šrámková (2009) and Fragile et al. (2016) have performed calculations of frequencies of the epicyclic oscillations of fluid tori assuming Kerr geometry, which describes rotating BHs. Here we follow their approach and consider slowly rotating NSs and their spacetimes described by the Hartle-Thorne geometry (Hartle, 1967; Hartle and Thorne, 1968). We present the first, preliminary results of our calculations of the radial epicyclic oscillation frequencies and provide a brief comparison of these to the frequencies obtained previously for the Kerr and linearized Kerr geometries. Finally, we discuss some consequences for models of NS QPOs.

## 2 OSCILLATIONS OF TORI IN AXIALLY SYMMETRIC SPACETIMES

We consider an axially symmetric geometry. The spacetime element may be expressed in the general form as

$$ds^2 = g_{tt}dt^2 + 2g_{t\varphi}dtd\varphi + g_{rr}dr^2 + g_{\theta\theta}d\theta^2 + g_{\varphi\varphi}d\varphi^2. \quad (1)$$

We use the units in which  $c = G = 1$  with  $c$  being the speed of light and  $G$  the gravitational constant.

### 2.1 Equilibrium configuration

We assume a perfect fluid torus in the state of pure rotation with constant specific angular momentum  $l$  as described in Abramowicz et al. (2006); Blaes et al. (2006).

In this case, the fluid forming the torus has a four-velocity  $u^\mu$  with only two non-zero components,

$$u^\mu = A(1, 0, 0, \Omega), \quad (2)$$

where  $A$  is the time component  $u^t$  and  $\Omega$  is the orbital velocity. One may write

$$A = u^t = (-g_{tt} - 2\Omega g_{t\varphi} - \Omega^2 g_{\varphi\varphi})^{-1/2}, \quad (3)$$

$$\Omega = \frac{u^\varphi}{u^t} = \frac{g^{t\varphi} - l g^{\varphi\varphi}}{g^{tt} - l g^{t\varphi}}. \quad (4)$$

<sup>1</sup> We often use the shorter term "QPOs" instead of "HF QPOs" throughout the paper.

The perfect fluid with density  $\rho$ , pressure  $p$  and the energy density  $e$  is characterised by the stress-energy tensor

$$T^{\mu\nu} = (p + e)u^\mu u^\nu + pg^{\mu\nu}. \quad (5)$$

For a polytropic fluid, we may write:

$$p = K\rho^{\frac{n+1}{n}}, \quad (6)$$

$$e = np + \rho, \quad (7)$$

where  $K$  and  $n$  denote the polytropic constant and the polytropic index, respectively. In this work, we use  $n = 3$ , which describes a radiation-pressure-dominated torus.

The Euler formula is obtained from the energy–momentum conservation law,  $\nabla_\mu T^\mu{}_\nu = 0$ , using the assumption of  $l = \text{const.}$  (Abramowicz et al., 1978, 2006)

$$\nabla_\mu(\ln \mathcal{E}) = -\frac{\nabla_\mu p}{p + e}, \quad (8)$$

with  $\mathcal{E}$  being the specific energy

$$\mathcal{E} = -u_t = \left(-g^{tt} + 2lg^{t\varphi} - l^2 g^{\varphi\varphi}\right)^{-1/2}. \quad (9)$$

By integrating (8) we obtain the Bernoulli equation (Fragile et al., 2016; Horák et al., 2017)

$$H\mathcal{E} = \text{const.}, \quad (10)$$

where  $H = \frac{p+e}{\rho}$  denotes the enthalpy in the form presented by Fragile et al. (2016) and Horák et al. (2017). From relation (10), we can derive the equations describing the structure and shape of the torus:

$$\frac{p}{\rho} = \frac{p_0}{\rho_0} f(r, \theta), \quad (11)$$

$$f(r, \theta) = \frac{1}{nc_{s,0}^2} \left[ \left(1 + nc_{s,0}^2\right) \frac{\mathcal{E}_0}{\mathcal{E}} - 1 \right], \quad (12)$$

$$(13)$$

where  $c_s$  is the sound speed in the fluid defined as (Abramowicz et al., 2006)<sup>2</sup>

$$c_s^2 = \frac{\partial p}{\partial \rho} = \frac{n+1}{n} \frac{p}{\rho}, \quad (14)$$

and the subscript 0 denotes the quantities evaluated at the torus centre. From equations (6) and (11), one can obtain the following formulae for pressure and density of the fluid:

$$p = p_0 [f(r, \theta)]^{n+1}, \quad (15)$$

$$\rho = \rho_0 [f(r, \theta)]^n. \quad (16)$$

<sup>2</sup> The definition is fully valid for  $c_s \ll 1$ , but this has no significant effect on our results.

It is useful to introduce new coordinates  $\bar{x}$  and  $\bar{y}$  by relations

$$\bar{x} = \frac{\sqrt{g_{rr,0}}}{\beta} \left( \frac{r - r_0}{r_0} \right), \quad (17)$$

$$\bar{y} = \frac{\sqrt{g_{\theta\theta,0}}}{\beta} \left( \frac{\frac{\pi}{2} - \theta}{r_0} \right). \quad (18)$$

In these coordinates, we have  $\bar{x} = 0$  and  $\bar{y} = 0$  at the torus centre. We furthermore introduce a  $\beta$  parameter determining the torus thickness, which is connected to the sound speed at the torus centre in the following manner (Abramowicz et al., 2006; Blaes et al., 2006):

$$\beta^2 = \frac{2nc_{s,0}^2}{r_0^2 \Omega_0^2 A_0^2}. \quad (19)$$

The surface of the torus, which coincides with the surface of zero pressure, is given by the condition  $f(r, \theta) = 0$ . An example of the torus cross-section is shown in Figure 1 illustrating the character of the equipressure surfaces for different values of  $\beta$ . An equilibrium torus is formed when the perfect fluid fills up a closed equipressure surface. The largest possible torus arises by filling up the equipressure surface that has a crossing point – the so-called cusp. We call this structure, for which we have  $\beta = \beta_{\text{cusp}}$ , the "cusp torus". Notice that, for  $\beta > \beta_{\text{cusp}}$ , the equipressure surfaces are no longer closed and no torus therefore can be formed.

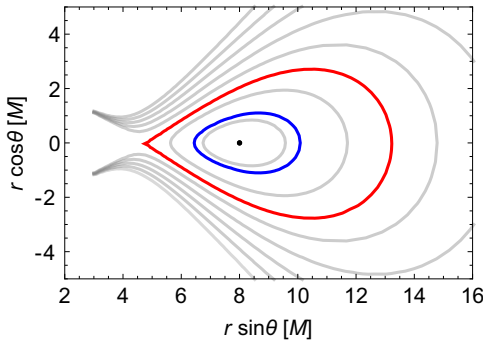


**Figure 1.** Meridional cross-section illustrating the shape of the equipressure surfaces in the Schwarzschild geometry. The red line marks a cusp torus with  $\beta = \beta_{\text{cusp}}$ , the blue line corresponds to an equilibrium torus with  $\beta < \beta_{\text{cusp}}$ , and the black dot denotes the centre of the torus (as well as the infinitely slender torus with  $\beta \rightarrow 0$ ).

## 2.2 The oscillating configuration

We assume the effective potential  $\mathcal{U}$  (e.g. Abramowicz et al., 2006) in the form

$$\mathcal{U} = g^{tt} - 2l_0 g^{t\varphi} + l_0^2 g^{\varphi\varphi}. \quad (20)$$

An infinitesimally slender torus with  $\beta \rightarrow 0$  at  $r_0$  with specific angular momentum  $l_0$  undergoing a small axially symmetric perturbation in the radial direction will oscillate with the frequency equal to the radial epicyclic frequency of a free test particle given by (Abramowicz and Kluźniak, 2005; Aliev and Galtsov, 1981)

$$v_r^2 = \frac{1}{4\pi^2} \frac{\mathcal{E}_0^2}{2A_0^2 g_{rr,0}} \left. \frac{\partial^2 \mathcal{U}}{\partial r^2} \right|_0. \quad (21)$$

Now let us investigate how the frequency changes when the torus becomes thicker and/or when the perturbation is not axially symmetric. Assume small perturbations of all quantities around the equilibrium state in the form (Abramowicz et al., 2006; Blaes et al., 2006)

$$\delta X(t, r, \theta, \varphi) = \delta X(r, \theta) e^{i(m\varphi - \omega t)}, \quad (22)$$

where  $m$  is the azimuthal number and  $\omega$  is the angular frequency of the oscillations. In this work, we focus on two modes of oscillations: the axially symmetric ( $m = 0$ ) and the first non-axisymmetric ( $m = -1$ ) radial epicyclic modes.

From the continuity equation  $\nabla_\mu (\rho u^\mu) = 0$ , one can get the relativistic version of the Papaloizou-Pringle equation (Abramowicz et al., 2006; Fragile et al., 2016),<sup>3</sup>

$$\begin{aligned} \frac{1}{\sqrt{-g}} \partial_\mu \frac{\sqrt{-g} g^{\mu\nu} f^n \partial_\nu W}{nc_{s,0}^2 f + 1} + (l_0 \omega - m)^2 \frac{\Omega g^{t\phi} - g^{\phi\phi}}{1 - \Omega l_0} \frac{f^n}{nc_{s,0}^2 f + 1} W = \\ = - \frac{2nA^2 (\bar{\omega} - m\bar{\Omega})^2}{\beta^2 r_0^2} f^{n-1} W, \end{aligned} \quad (23)$$

where  $\{\mu, \nu\} \in \{r, \theta\}$ ,  $\mathcal{A} \equiv A/A_0$ ,  $\bar{\Omega} \equiv \Omega/\Omega_0$ ,  $\bar{\omega} \equiv \omega/\Omega_0$ ,  $g$  is the determinant of the metric tensor and  $W$  equals to (Abramowicz et al., 2006)

$$W = - \frac{\delta p}{A\rho(\omega - m\Omega)}. \quad (24)$$

Equation (23) has no analytical solution except for the limit case of an infinitely slender torus ( $\beta \rightarrow 0$ ). In the case of non-slender tori ( $\beta > 0$ ), the equation can be solved using a perturbation method (see, e.g., Straub and Šrámková (2009)).

### 2.2.1 Solving the Papaloizou-Pringle equation

When the exact solution for a simplified case is known (as for  $\beta \rightarrow 0$ ), we can use perturbation theory to find the solution for more complicated cases ( $\beta > 0$ ).<sup>4</sup>

<sup>3</sup> For the sake of simplicity, from now on, we will use  $f = f(r, \theta)$ .

<sup>4</sup> Note the perturbation method gives reasonable results only for small values of  $\beta$  and our results are therefore valid only for slightly non-slender tori.

By expanding the quantities  $\bar{\omega}$ ,  $W$ ,  $\mathcal{A}$ ,  $\bar{\Omega}$ ,  $f$  in  $\beta$  (Straub and Šrámková, 2009)

$$Q = Q^{(0)} + \beta Q^{(1)} + \beta^2 Q^{(2)} + \dots, \quad Q \in \{\bar{\omega}, W, \mathcal{A}, \bar{\Omega}, f\}, \quad (25)$$

substituting that into equation (23), and comparing the coefficients of appropriate order in  $\beta$ , we obtain the corresponding corrections to  $W$  and  $\omega$ . Note that the zero order corresponds to the slender torus case ( $\beta \rightarrow 0$ ), in which we have  $\omega = 2\pi\nu_r$ .

Using this procedure, Straub and Šrámková (2009) have derived the expression for the radial epicyclic mode frequency with the second order accuracy, which may be written as

$$\omega_{r,m} = 2\pi\nu_r + m\Omega_0 + P_m\beta^2 + \mathcal{O}(\beta^3), \quad (26)$$

where  $P_m$  denotes the second order correction term for which the explicit form can be found in their paper.

### 3 THE HARTLE-THORNE GEOMETRY

The exterior solution of the Hartle-Thorne metric is characterized by three parameters: the gravitational mass  $M$ , angular momentum  $J$  and the quadrupole moment  $Q$  of the star. We use this metric assuming dimensionless forms of the angular momentum and the quadrupole moment,  $j = J/M^2$  and  $q = Q/M^3$ , which can be in the Schwarzschild coordinates written as (Abramowicz et al., 2003)<sup>5</sup>:

$$g_{tt} = -\left(1 - \frac{2M}{r}\right) \left[1 + j^2 F_1(r) + q F_2(r)\right], \quad (27)$$

$$g_{rr} = \left(1 - \frac{2M}{r}\right)^{-1} \left[1 + j^2 G_1(r) - q F_2(r)\right], \quad (28)$$

$$g_{\theta\theta} = r^2 \left[1 + j^2 H_1(r) + q H_2(r)\right], \quad (29)$$

$$g_{\varphi\varphi} = r^2 \sin^2 \theta \left[1 + j^2 H_1(r) + q H_2(r)\right], \quad (30)$$

$$g_{t\varphi} = -\frac{2M^2}{r} j \sin^2 \theta, \quad (31)$$

where (using the  $u = \cos \theta$  substitution)

$$F_1(r) = -\left[8Mr^4(r-2M)\right]^{-1} \left[ u^2 (48M^6 - 8M^5r - 24M^4r^2 - 30M^3r^3 - 60M^2r^4 + 135Mr^5 - 45r^6) + (r-M) (16M^5 + 8M^4r - 10M^2r^3 - 30Mr^4 + 15r^5) \right] + A_1(r), \quad (32)$$

<sup>5</sup> Note misprints in the original paper.

$$F_2(r) = [8Mr(r-2M)]^{-1} \left[ 5(3u^2-1)(r-M)(2M^2+6Mr-3r^2) \right] - A_1(r), \quad (33)$$

$$G_1(r) = [8Mr(r-2M)]^{-1} \left[ (L(r)-72M^5r) - 3u^2(L(r)-56M^5r) \right] - A_1(r), \quad (34)$$

$$L(r) = 80M^6 + 8M^4r^2 + 10M^3r^3 + 20M^2r^4 - 45Mr^5 + 15r^6, \quad (35)$$

$$A_1(r) = \frac{15(r^2-2M)(1-3u^2)}{16M^2} \ln\left(\frac{r}{r-2M}\right), \quad (36)$$

$$H_1(r) = (8Mr^4)^{-1} (1-3u^2) (16M^5 + 8M^4r - 10M^2r^3 + 15Mr^4 + 15r^5) + A_2(r), \quad (37)$$

$$H_2(r) = (8Mr)^{-1} 5(1-3u^2) (2M^2 - 3Mr - 3r^2) - A_2(r), \quad (38)$$

$$A_2(r) = \frac{15(r^2-2M)(3u^2-1)}{16M^2} \ln\left(\frac{r}{r-2M}\right). \quad (39)$$

While for  $j = 0$  and  $q = 0$  the Hartle-Thorne metric coincides with the Schwarzschild metric, by setting  $j = a/M$  and  $q = j^2$  and performing a coordinate transformation into the Boyer-Lindquist coordinates (Abramowicz et al., 2003),

$$r_{\text{BL}} = r - \frac{a^2}{2r^3} \left[ (r+2M)(r-2M) + u^2(r-2M)(r+3M) \right], \quad (40)$$

$$\theta_{\text{BL}} = \theta - \frac{a^2}{2r^3} (r+2M) \cos\theta \sin\theta, \quad (41)$$

we obtain Kerr geometry expanded upon the second order in the dimensionless angular momentum.

## 4 OSCILLATIONS OF TORI IN THE VICINITY OF ROTATING NEUTRON STARS

Let us now study the changes that arise in the torus structure and for the frequencies of its oscillations when the Hartle-Thorne geometry is assumed to describe the spacetime geometry.<sup>6</sup> The main motivation behind this analysis is related to models of NS QPOs. While the Kerr geometry is (likely) proper to be used in the context of BH QPOs (e.g., Kotrlová et al., 2020), its validity in the case of NS QPOs is limited to very compact NSs only.

### 4.1 The Hartle-Thorne geometry parameters range relevant to rotating NSs

A thorough discussion of the relevance of the Hartle-Thorne geometry for the calculations of the geodesic orbital motion and QPO models frequencies is presented in Urbancová et al. (2019). Here we just briefly summarize the appropriate ranges of the individual parameters that are implied by the present NS equations of state. The maximum value of the specific

<sup>6</sup> Following Straub and Šrámková (2009) and Fragile et al. (2016), we use a Wolfram Mathematica code, which has been extended to the Hartle-Thorne geometry.

angular momentum of a NS is about  $j_{\max} \sim 0.7$ , the specific quadrupole moment takes values from  $q/j^2 \sim 1.5$  for a very massive (compact) NS up to  $q/j^2 \sim 10$  for a low-mass NS (Urbancová et al., 2019). The conservative expectations of the NS mass values are about  $1.4 - 2.5 M_{\odot}$ .

## 4.2 The quadrupole moment influence on the non-oscillating torus shape and size

In Figures 2 and 3, we present meridional cross-sections of tori carried out in different geometries, namely the Schwarzschild, Kerr, linearized Kerr, and the Hartle-Thorne geometry. The figures also show plots of the Keplerian angular momentum and the angular momentum of the fluid (which is constant across the torus), and the radial extensions of the tori. For both figures, the top panels correspond to  $j = 0$  (a non-rotating NS, i.e., the Schwarzschild geometry), and the bottom panels to  $j = 0.2$  (Figure 2) and  $j = 0.4$  (Figure 3). The radial coordinate  $r_0$  is chosen such that the radial epicyclic frequency of a free test particle defined at this coordinate reaches its maximum.

In Table 1, we provide a quantitative comparison of the radial extensions of tori from Figures 2 and 3. It is given in terms of the proper radial distance,  $r_{\text{prop}}$ , measured between the minimal,  $r_{\min}$ , and the maximal,  $r_{\max}$ , radial coordinate of the torus surface,

$$\Delta r_{\text{prop}} = \int_{r_{\min}}^{r_{\max}} \sqrt{g_{rr}} dr. \quad (42)$$

**Table 1.** The percentual differences in the proper radial extension  $\Delta r_{\text{prop}}$  of tori in the Hartle-Thorne geometry and in the Schwarzschild, Kerr, and linearized Kerr geometries. The displayed values correspond to the situations illustrated in Figures 2 and 3.

Geometry	Schwarzschild		Kerr		Lin. Kerr	
	0.2	0.4	0.2	0.4	0.2	0.4
Spin $j$						
HT ( $q = j^2$ )	-5 %	-11 %	+2 %	-5 %	-1 %	-13 %
HT ( $q = 10j^2$ )	-7 %	-12 %	-1 %	-6 %	-4 %	-14 %

## 4.3 The quadrupole moment influence on the radial epicyclic oscillations of non-slender tori

We use equation (26) to derive the radial epicyclic mode frequency as a function of the radius of the torus centre  $r_0$ . In Figure 4, we plot the frequencies of both the  $m = 0$  (left panel) and  $m = -1$  (middle panel) radial epicyclic modes. These are compared for the four different geometries assuming  $j = 0.2$ . The right panel of this figure illustrates the behaviour of tori cross-sections corresponding to maxima of the  $m = 0$  radial epicyclic mode frequency. Figure 5 then provides the same illustration but for  $j = 0.4$ .



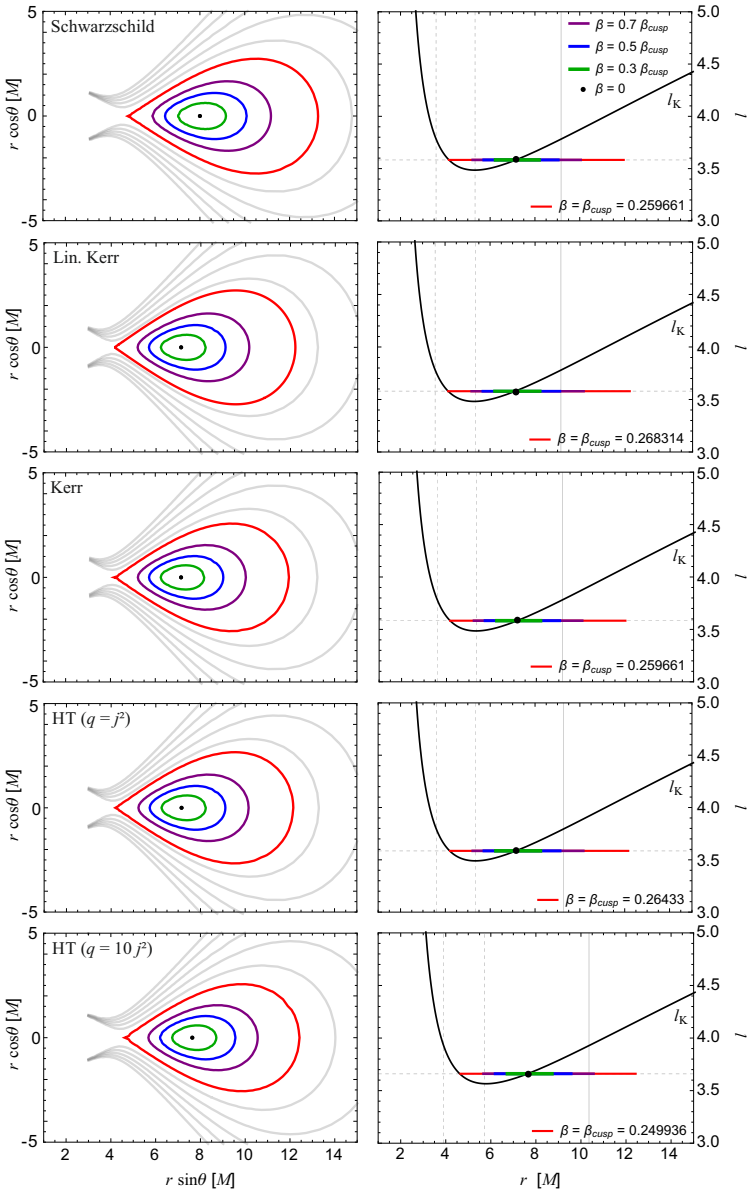


**Figure 2.** Illustration of some characteristics of tori carried out in different geometries. The tori are centered at the radial coordinate at which the radial epicyclic frequency of a free test particle reaches its maximum. Left panels: Meridional cross-sections of the equipressure surfaces determining the shape of the tori. From top to bottom, the results correspond to calculations carried out in the Schwarzschild, linearized Kerr ( $j = 0.2$ ), Kerr ( $j = 0.2$ ), and the Hartle-Thorne ( $j = 0.2, q = j^2$  and  $j = 0.2, q = 10j^2$ ) geometry. Right panels: Plots of the specific angular momentum of the fluid (which is constant across the torus) along with the Keplerian angular momentum. The intersection points of the two functions marked by the spots correspond to the centre of the tori. The coloured segments indicate the corresponding radial extensions of the tori.

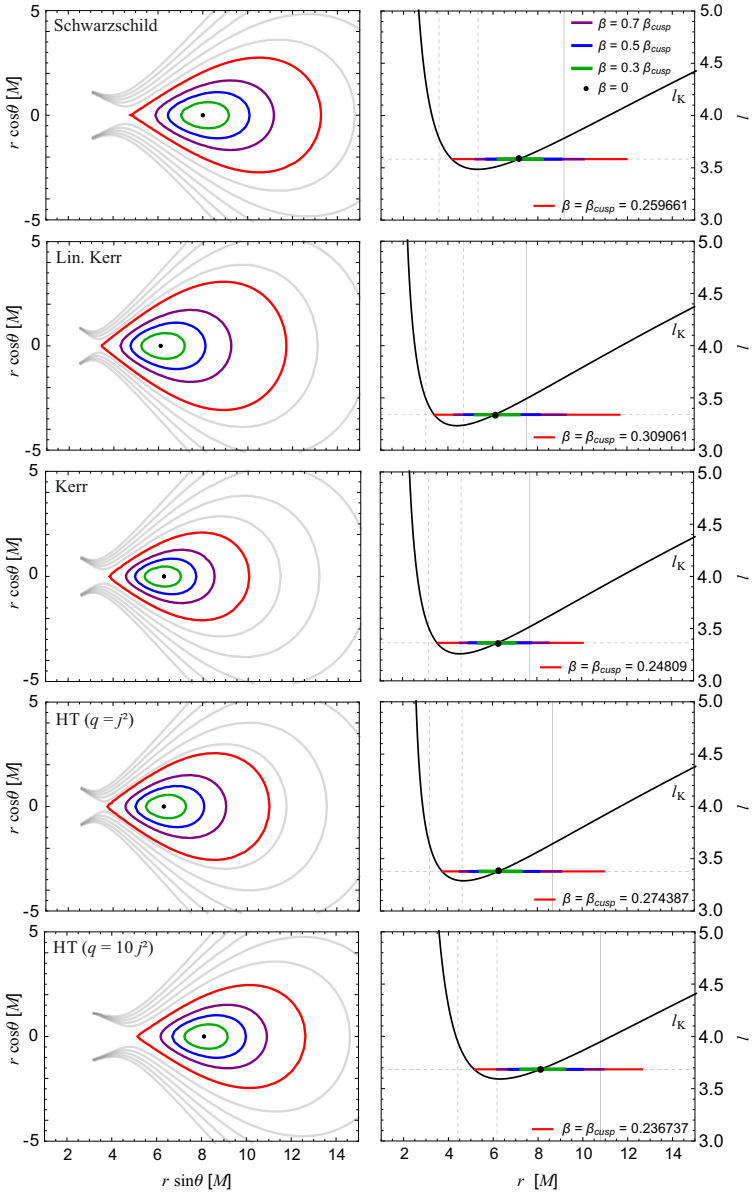


**Figure 3.** The same as in Figure 2 but for  $j = 0.4$ .

In Table 2, we provide a quantitative comparison of the maximal frequencies of the  $m = 0$  radial epicyclic mode for tori of maximal thicknesses (i.e., the frequencies denoted by the red dots in the left panels of Figures 4 and 5) for the Hartle-Thorne and the other three geometries. In Table 3, we then present the same but for the  $m = -1$  radial epicyclic mode (i.e., the frequencies denoted by the red dots in the middle panels of Figures 4 and 5). The proper radial extension of tori related to Tables 2 and 3 (i.e., those shown in the right panels of Figures 4 and 5) are compared in Table 4.

**Table 2.** The percentual differences in the maximal values of frequencies of the  $m = 0$  radial epicyclic mode of the cusp tori in the Hartle-Thorne geometry and in the Schwarzschild, Kerr, and linearized Kerr geometries. The displayed values correspond to the situations illustrated in Figures 4 and 5.

Geometry	Schwarzschild		Kerr		Lin. Kerr	
	0.2	0.4	0.2	0.4	0.2	0.4
Spin $j$						
HT ( $q = j^2$ )	+ 15 %	+ 35 %	0 %	0 %	- 1 %	- 4 %
HT ( $q = 10j^2$ )	+ 8 %	+ 4 %	- 6 %	- 23 %	- 7 %	- 26 %

**Table 3.** The percentual differences in the frequency of the  $m = -1$  radial epicyclic mode of the cusp tori in the Hartle-Thorne geometry and in the Schwarzschild, Kerr, and linearized Kerr geometries. The frequency is evaluated at the radius at which the  $m = 0$  radial epicyclic mode frequency has its maximum. The displayed values correspond to the situations illustrated in Figures 4 and 5.

Geometry	Schwarzschild		Kerr		Lin. Kerr	
	0.2	0.4	0.2	0.4	0.2	0.4
Spin $j$						
HT ( $q = j^2$ )	+ 20 %	+ 49 %	0 %	- 1 %	- 1 %	- 8 %
HT ( $q = 10j^2$ )	+ 5 %	- 10 %	- 23 %	- 40 %	- 14 %	- 44 %

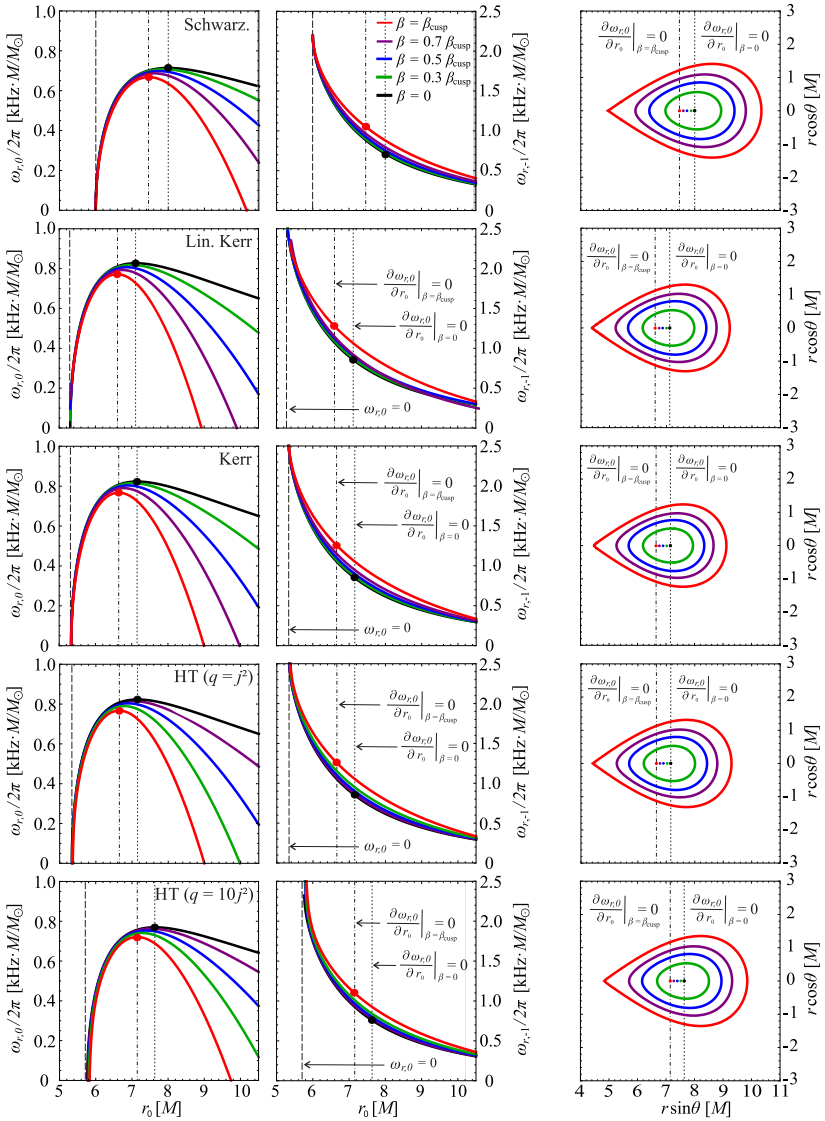


**Figure 4.** Frequencies of the radial epicyclic mode.

Left panels: The  $m = 0$  case. From top to bottom: the Schwarzschild, linearized Kerr, Kerr, and the Hartle-Thorne ( $q = j^2$  and  $q = 10j^2$ ) geometry. For rotating stars, we assume  $j = 0.2$ . The maximal frequencies allowed for the slender torus and for the cusp torus are denoted by the black and red spots, respectively.

Middle panels: The same but for the  $m = -1$  case. The coloured spots denote the frequency value corresponding to the radius at which the  $m = 0$  radial mode frequency has its maximum.

Right panels: Tori that would oscillate with the maximal value of the  $m = 0$  radial epicyclic mode frequency for a given torus thickness.

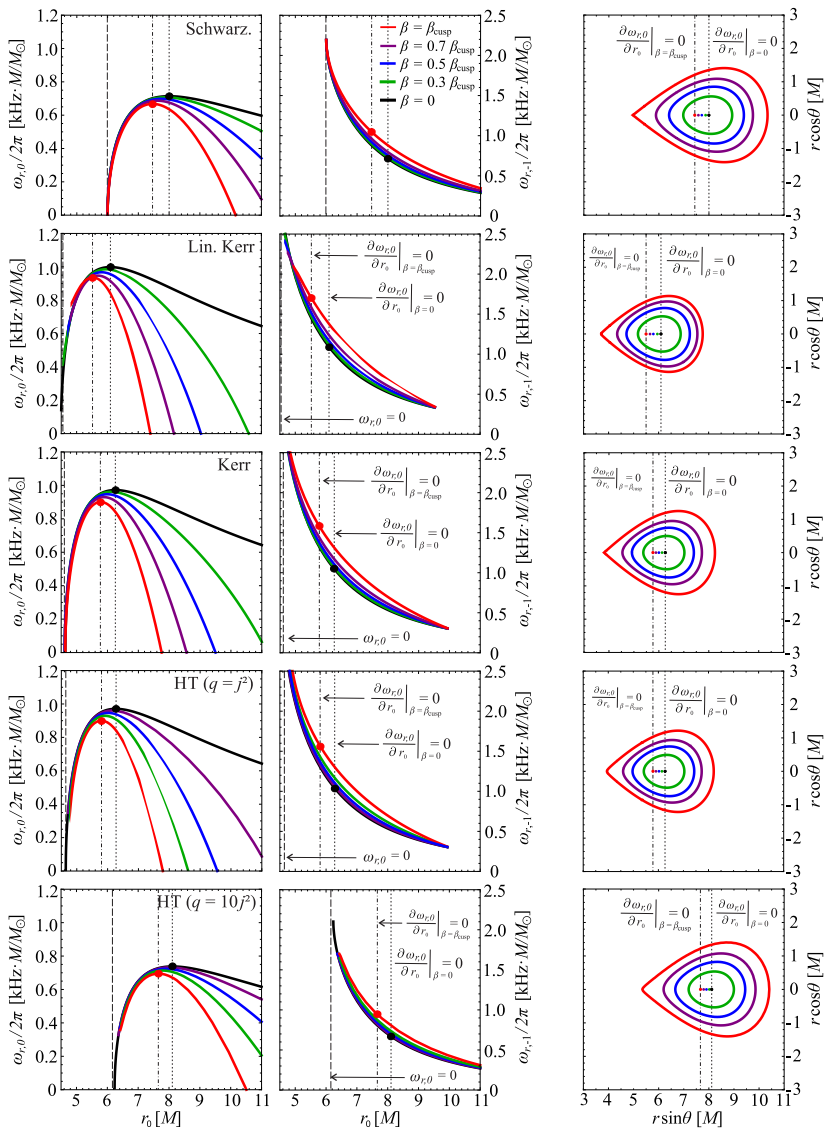
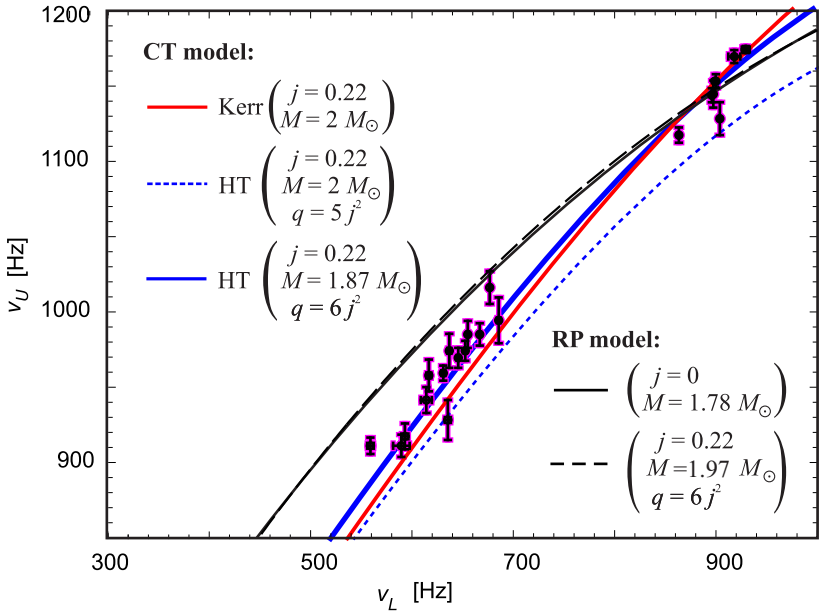


Figure 5. The same as in Figure 4 but for  $a = 0.4$ .

**Table 4.** The percentual differences in the proper radial extension  $\Delta r_{\text{prop}}$  of the cusp tori relevant to Tables 2 and 3 and shown in the right panels of Figures 4 and 5.

Geometry	Schwarzschild		Kerr		Lin. Kerr	
Spin $j$	0.2	0.4	0.2	0.4	0.2	0.4
HT ( $q = j^2$ )	-7 %	-17 %	0 %	-4 %	0 %	+1 %
HT ( $q = 10j^2$ )	-6 %	-7 %	-4 %	+7 %	+2 %	+13 %

**Figure 6.** Frequency correlations predicted by the CT model vs. data of the 4U 1636-53 atoll source. The fit for  $j = 0.22$  obtained under the consideration of the Kerr geometry (the curve marked as Kerr) is compared here to two examples of predictions obtained under the consideration of the Hartle-Thorne geometry (the curves marked as HT). Examples of the best fits predicted by the relativistic precession model for a given  $j$  and  $q$  are shown as well (the curves marked as RP model).

## 5 DISCUSSION AND CONCLUSIONS

Our results indicate that, while the shape of the non-oscillating tori is not much sensitive to the NS quadrupole moment, the frequencies of the radial epicyclic modes of tori oscillations are affected significantly. Clearly, the difference of the frequencies of oscillations

of tori around BHs and NSs can reach tens of percents. Although a more detailed analysis is certainly needed (including the completion of the radial epicyclic mode investigation as well as the investigation of the vertical epicyclic mode behaviour), we may already conclude that the consideration of the quadrupole moment induced by the NS rotation likely should have an impact on the modeling of the high-frequency quasi-periodic oscillations.

Our conclusion is demonstrated in Figure 6. There we consider a recently proposed QPO model (CT model; Török et al., 2016a) and compare the frequencies predicted by the model for several combinations of  $M$ ,  $j$ ,  $q$  with the frequencies observed in the 4U 1636-53 atoll source (the data are taken from Barret et al., 2006; Török, 2009). We include in the figure examples of correlations predicted by the relativistic precession model (Stella and Vietri, 1999). This model provides less promising fits of the data than the CT model while the effects associated to the NS rotation do not imply a significant improvement (see Török et al., 2012; Török et al., 2016b,a). It is clear from the figure that even when we restrict ourselves to values of the Hartle-Thorne spacetime parameters that are consistent with up-to-date models of neutron stars, no conceivable smooth curve can reproduce the data in a significantly better way compared to the CT model.

## ACKNOWLEDGEMENTS

We acknowledge two internal grants of the Silesian University, SGS/12, 13/2019. We wish to thank the INTER-EXCELLENCE project No. LTI17018. KK thanks to the INTER-EXCELLENCE project No. LTT17003. DL thanks the Student Grant Foundation of the Silesian University in Opava, Grant No. SGF/1/2020, which has been carried out within the EU OPSRE project entitled “Improving the quality of the internal grant scheme of the Silesian University in Opava”, reg. number: CZ.02.2.69/0.0/0.0/19\_073/0016951. The authors were also supported by the ESF projects No. CZ.02.2.69/0.0/0.0/18\_054/0014696.

## REFERENCES

- Abramowicz, M., Jaroszynski, M. and Sikora, M. (1978), Relativistic, accreting disks, *Astronomy and Astrophysics*, **63**, pp. 221–224.
- Abramowicz, M. A., Almergren, G. J. E., Kluzniak, W. and Thampan, A. V. (2003), The hartle-thorne circular geodesics, [arXiv: gr-qc/0312070v1](https://arxiv.org/abs/gr-qc/0312070v1).
- Abramowicz, M. A., Blaes, O. M., Horák, J., Kluzniak, W. and Rebusco, P. (2006), Epicyclic oscillations of fluid bodies: II. Strong gravity, *Classical and Quantum Gravity*, **23**, pp. 1689–1696, [arXiv: astro-ph/0511375](https://arxiv.org/abs/astro-ph/0511375).
- Abramowicz, M. A., Bulik, T., Bursa, M. and Kluzniak, W. (2003a), Evidence for a 2:3 resonance in Sco X-1 kHz QPOs, *A&A*, **404**, pp. L21–L24, [arXiv: astro-ph/0206490](https://arxiv.org/abs/astro-ph/0206490).
- Abramowicz, M. A., Karas, V., Kluzniak, W., Lee, W. H. and Rebusco, P. (2003b), Non-Linear Resonance in Nearly Geodesic Motion in Low-Mass X-Ray Binaries, *PAS*, **55**, pp. 467–466, [arXiv: astro-ph/0302183](https://arxiv.org/abs/astro-ph/0302183).
- Abramowicz, M. A. and Kluzniak, W. (2005), Epicyclic Frequencies Derived From The Effective Potential: Simple And Practical Formulae, *Astrophysics and Space Science*, **300**, pp. 127–136, [arXiv: astro-ph/0411709](https://arxiv.org/abs/astro-ph/0411709).

- Aliev, A. N. and Galtsov, D. V. (1981), Radiation from relativistic particles in nongeodesic motion in a strong gravitational field, *General Relativity and Gravitation*, **13**, pp. 899–912.
- Barret, D., Olive, J.-F. and Miller, M. C. (2006), The coherence of kilohertz quasi-periodic oscillations in the X-rays from accreting neutron stars, *MNRAS*, **370**, pp. 1140–1146, [arXiv: astro-ph/0605486](#).
- Blaes, O. M., Arras, P. and Fragile, P. C. (2006), Oscillation modes of relativistic slender tori, *Monthly Notices of the Royal Astronomical Society*, **369**, pp. 1235–1252, [arXiv: astro-ph/0601379](#).
- Bursa, M. (2005), Global oscillations of a fluid torus as a modulation mechanism for black-hole high-frequency QPOs, *Astronomische Nachrichten*, **326**(9), pp. 849–855, [arXiv: astro-ph/0510460](#).
- de Avellar, M. G. B., Porth, O., Younsi, Z. and Rezzolla, L. (2018), Kilohertz QPOs in low-mass X-ray binaries as oscillation modes of tori around neutron stars - I, *MNRAS*, **474**, pp. 3967–3975.
- Dönmez, O., Zanotti, O. and Rezzolla, L. (2011), On the development of quasi-periodic oscillations in Bondi-Hoyle accretion flows, *MNRAS*, **412**(3), pp. 1659–1668, [arXiv: 1010.1739](#).
- Fragile, P. C., Straub, O. and Blaes, O. (2016), High-frequency and type-c QPOs from oscillating, precessing hot, thick flow, *Monthly Notices of the Royal Astronomical Society*, **461**(2), pp. 1356–1362.
- Hartle, J. B. (1967), Slowly Rotating Relativistic Stars. I. Equations of Structure, *APJL*, **150**, p. 1005.
- Hartle, J. B. and Thorne, K. S. (1968), Slowly Rotating Relativistic Stars. II. Models for Neutron Stars and Supermassive Stars, *APJ*, **153**, p. 807.
- Horák, J., Straub, O., Šrámková, E., Goluchová, K. and Török, G. (2017), Epicyclic oscillations of thick relativistic disks, in *RAGtime 17-19: Workshops on Black Holes and Neutron Stars*, pp. 47–59, URL <https://ui.adsabs.harvard.edu/abs/2017bhns.work...47H>.
- Kluźniak, W. and Abramowicz, M. A. (2001), The physics of kHz QPOs—strong gravity’s coupled anharmonic oscillators, *arXiv e-prints*, astro-ph/0105057, [arXiv: astro-ph/0105057](#).
- Kluźniak, W., Abramowicz, M. A., Kato, S., Lee, W. H. and Stergioulas, N. (2004), Nonlinear Resonance in the Accretion Disk of a Millisecond Pulsar, *APJL*, **603**(2), pp. L89–L92, [arXiv: astro-ph/0308035](#).
- Kotrllová, A., Šrámková, E., Török, G., Goluchová, K., Horák, J., Straub, O., Lančová, D., Stuchlík, Z. and Abramowicz, M. A. (2020), Models of high-frequency quasi-periodic oscillations and black hole spin estimates in Galactic microquasars, *A&A*, **643**, A31, [arXiv: 2008.12963](#).
- Rezzolla, L., Yoshida, S. and Zanotti, O. (2003), Oscillations of vertically integrated relativistic tori - I. Axisymmetric modes in a Schwarzschild space-time, *MNRAS*, **344**, pp. 978–992, [arXiv: astro-ph/0307488](#).
- Stella, L. and Vietri, M. (1999), kHz Quasiperiodic Oscillations in Low-Mass X-Ray Binaries as Probes of General Relativity in the Strong-Field Regime, *PRL*, **82**(1), pp. 17–20, [arXiv: astro-ph/9812124](#).
- Straub, O. and Šrámková, E. (2009), Epicyclic oscillations of non-slender fluid tori around Kerr black holes, *Classical and Quantum Gravity*, **26**(5), 055011, [arXiv: 0901.1635](#).
- Török, G. (2009), Reversal of the amplitude difference of kHz QPOs in six atoll sources, *A&A*, **497**, pp. 661–665, [arXiv: 0812.4751](#).
- Török, G., Abramowicz, M. A., Kluźniak, W. and Stuchlík, Z. (2005), The orbital resonance model for twin peak kHz quasi periodic oscillations in microquasars, *A&A*, **436**, pp. 1–8.
- Török, G., Bakala, P., Šrámková, E., Stuchlík, Z., Urbanec, M. and Goluchová, K. (2012), Mass-angular-momentum relations implied by models of twin peak quasi-periodic oscillations, [arXiv: 1408.4220v1](#).
- Török, G., Goluchová, K., Horák, J., Šrámková, E., Urbanec, M., Pecháček, T. and Bakala, P. (2016a), Twin peak quasi-periodic oscillations as signature of oscillating cusp torus, *MNRAS*, **457**, pp. L19–



L23, [arXiv: 1512.03841](#).

Török, G., Goluchová, K., Urbanec, M., Šrámková, E., Adámek, K., Urbancová, G., Pecháček, T., Bakala, P., Stuchlík, Z., Horák, J. and Juryšek, J. (2016b), Constraining Models of Twin-Peak Quasi-periodic Oscillations with Realistic Neutron Star Equations of State, *The Astrophysical Journal*, **833**, 273, [arXiv: 1611.06087](#).

Urbancová, G., Urbanec, M., Török, G., Stuchlík, Z., Blaschke, M. and Miller, J. C. (2019), Epicyclic Oscillations in the Hartle-Thorne External Geometry, *The Astrophysical Journal*, **877**(2), 66, [arXiv: 1905.00730](#).